Woronin body hitchhiking on early endosomes is dispensable for septal localization in *Aspergillus nidulans*

Livia D. Songster[a], Devahuti Bhuyan[b], Jenna R. Christensen[b,*], and Samara L. Reck-Peterson[a,b,c,*]
[a]Department of Cell and Developmental Biology and [b]Department of Cellular and Molecular Medicine, University of California, San Diego, La Jolla, CA 92093; [c]Howard Hughes Medical Institute, Chevy Chase, MD 20815

ABSTRACT **The proper functioning of organelles depends on their intracellular localization, mediated by motor protein–dependent transport on cytoskeletal tracks. Rather than directly associating with a motor protein, peroxisomes move by hitchhiking on motile early endosomes in the filamentous fungus *Aspergillus nidulans*. However, the physiological role of peroxisome hitchhiking is unclear. Peroxisome hitchhiking requires the protein PxdA, which is conserved within the fungal subphylum Pezizomycotina but absent from other fungal clades. Woronin bodies are specialized peroxisomes that are also unique to the Pezizomycotina. In these fungi, multinucleate hyphal segments are separated by incomplete cell walls called septa that possess a central pore enabling cytoplasmic exchange. Upon damage to a hyphal segment, Woronin bodies plug septal pores to prevent widespread leakage. Here, we tested whether peroxisome hitchhiking is important for Woronin body motility, distribution, and function in *A. nidulans*. We show that Woronin body proteins are present within all motile peroxisomes and hitchhike on PxdA-labeled early endosomes during bidirectional, long-distance movements. Loss of peroxisome hitchhiking significantly affected Woronin body distribution and motility in the cytoplasm, but Woronin body hitchhiking is ultimately dispensable for septal localization and plugging.**

Monitoring Editor
Anne Spang
University of Basel

Received: Jan 30, 2023
Revised: Mar 28, 2023
Accepted: Mar 28, 2023

INTRODUCTION

Within a eukaryotic cell, organelles are precisely positioned to regulate their cellular function. The intracellular trafficking of these cargoes is primarily achieved by molecular motors that bind different cargoes and directly transport them along cytoskeletal filaments like microtubules or actin (Reck-Peterson *et al.*, 2018; Titus, 2018). Microtubules are polar structures that serve as the primary track for transporting cargo long distances in eukaryotes. They possess a fast-growing plus end typically oriented toward the cell periphery and a minus end originating at a microtubule-organizing center. Kinesin motors transport cargo predominantly toward the plus end of microtubules (anterograde) (Hirokawa *et al.*, 2009). Conversely, cytoplasmic dynein motors ("dynein" here) transport cargo toward microtubule minus ends (retrograde) (Reck-Peterson *et al.*, 2018).

The canonical view of intracellular transport is that a cargo attaches directly to a motor protein for movement, typically via a protein adaptor (Reck-Peterson *et al.*, 2018; Olenick and Holzbaur, 2019). However, a novel form of intracellular transport termed "hitchhiking" was recently discovered, whereby a primary cargo directly interacts with a motor and a secondary hitchhiking cargo is transported indirectly via association with the primary cargo (Christensen and Reck-Peterson, 2022). Hitchhiking-like phenomena have been observed in diverse cell types and organisms such as filamentous fungi (Guimaraes *et al.*, 2015; Salogiannis *et al.*, 2016), animal neurons (Özkan *et al.*, 2021; Harbauer *et al.*, 2022), and plant cells (Oikawa *et al.*, 2003; Luo *et al.*, 2022).

This article was published online ahead of print in MBoC in Press (http://www.molbiolcell.org/cgi/doi/10.1091/mbc.E23-01-0025) on April 5, 2023.

Author contributions: L.D.S., J.R.C., and S.L.R-P. devised the experiments. L.D.S. and D. B. performed the experiments. J.R.C. and S.L.R-P. supervised the research. L.D.S., J.R.C., and S.L.R-P. wrote and edited the manuscript.

*Address correspondence to: Jenna R. Christensen (jrc039@health.ucsd.edu) and Samara L. Reck-Peterson (sreckpeterson@ucsd.edu).

Abbreviations used: DipA, DenA-interacting phosphatase A; PxdA, peroxisome distribution mutant A.

In *Aspergillus nidulans*, peroxisomes move long distances along microtubules by hitchhiking on motile early endosomes transported by kinesin-3 or dynein (Salogiannis *et al.*, 2016). We previously identified a putative molecular tether (peroxisome distribution mutant A; PxdA) and a phosphatase (DenA-interacting phosphatase A; DipA) that are essential for peroxisome hitchhiking on early endosomes (Salogiannis *et al.*, 2021). Both PxdA and DipA are found on early endosomes, and loss of either compromises long-distance motility of peroxisomes, resulting in an accumulation of peroxisomes in the hyphal tip without affecting early endosome motility or distribution (Salogiannis *et al.*, 2016, 2021). Peroxisomes are the only organelle demonstrated to hitchhike on early endosomes in *A. nidulans* (Salogiannis *et al.*, 2021), but the physiological role for why peroxisomes hitchhike is unclear.

Using comparative genomics, we found that PxdA is conserved within the Pezizomycotina subphylum of ascomycete filamentous fungi, suggesting that a function for peroxisome hitchhiking might also be conserved within this clade. We therefore investigated whether hitchhiking was required for septal plugging, a peroxisome function unique to the Pezizomycotina.

Septal plugging is a critical process within Pezizomycotina fungi as they possess continuous hyphal compartments separated only by a septal wall containing a pore (Mouriño-Pérez, 2013). This interconnected hyphal network or "mycelium" has the advantage of quickly exchanging components throughout the organism (Bleichrodt *et al.*, 2012; Tegelaar and Wösten, 2017). However, if one portion of the organism is injured or lysed, significant cytoplasmic leakage can occur. In many species within the Pezizomycotina, peroxisome derivatives known as Woronin bodies plug septal pores upon mycelial injury, allowing the rest of the mycelium to remain intact (Jedd and Chua, 2000). Woronin bodies can also function to dynamically open and close pores to control hyphal heterogeneity (Bleichrodt *et al.*, 2012). Woronin body biogenesis is thought to initiate at the growing hyphal tip, based on a spatial bias in mRNA expression of the essential Woronin body component Hex-1 in *Neurospora crassa* (Tey *et al.*, 2005). After biogenesis at the hyphal tip, Woronin bodies are hypothesized to be transported to nascent septal sites, where they bud from peroxisomes and remain tethered at the septa (Momany *et al.*, 2002; Leonhardt *et al.*, 2017). However, the mechanism by which Woronin bodies are transported to septa is unknown.

In this study, we investigated whether peroxisome hitchhiking is important for Woronin body motility, positioning, and function in *A. nidulans*. We find that Woronin body proteins associated with peroxisomes move dynamically and bidirectionally and that this motility is dependent on PxdA-mediated hitchhiking on early endosomes. We show that Woronin bodies separate from peroxisomes once localized to septa but this fission process does not require PxdA. Finally, we show that the distribution of Woronin bodies in hyphal tips requires hitchhiking but this is ultimately dispensable for both the positioning of Woronin bodies at septa and their function in septal closure after hyphal injury.

RESULTS AND DISCUSSION

Peroxisome hitchhiking proteins and Woronin body specialization are conserved within the Pezizomycotina fungi

Peroxisome hitchhiking has been directly observed in two species of fungi, *A. nidulans* and *Ustilago maydis* (Guimaraes *et al.*, 2015; Salogiannis *et al.*, 2016). However, a physiological function for peroxisome hitchhiking has not been established. Two early endosome-associated proteins, a putative molecular tether (PxdA) and a phosphatase (DipA), have been shown to be essential for peroxisome hitchhiking in *A. nidulans* (Salogiannis *et al.*, 2016, 2021).

To gain insight into the physiological role for peroxisome hitchhiking, we used comparative genomics to identify which fungal clades likely exhibit PxdA-dependent peroxisome hitchhiking. We used BLASTp to search for DipA and PxdA protein homologues in 33 fungal species representing distinct clades across the fungal tree (Supplemental Figure S1, A–C), with the underlying assumption that fungal species encoding both PxdA and DipA in their genomes would exhibit peroxisome hitchhiking. Putative PxdA homologues were identified only in the Pezizomycotina clade and were present in all 15 Pezizomycotina species that we analyzed (Supplemental Figure S1C; Supplemental Table S1). We previously identified a point mutation in PxdA (R2044P) that abolishes its association with early endosomes and subsequent peroxisome hitchhiking (Salogiannis *et al.*, 2021). We performed multiple sequence alignments on identified PxdA homologues, revealing that amino acid R2044 is present in all 15 homologues that we examined and exists within a highly conserved patch of hydrophilic amino acids (Supplemental Figure S1D).

Peroxisome hitchhiking has also been observed outside of the Pezizomycotina, in the basidiomycete *U. maydis* (Guimaraes *et al.*, 2015). We did not identify a homologue of PxdA in *U. maydis*, suggesting that peroxisome hitchhiking may function by a distinct mechanism in this species. However, it is possible that *U. maydis* possesses a PxdA homologue that is sequence divergent and therefore not identified by our methods.

Putative DipA homologues were identified in all queried Pezizomycotina species as well as in other fungal clades (Supplemental Table S1). DipA functions in cellular processes beyond peroxisome hitchhiking, including septal positioning (Schinke *et al.*, 2016), likely explaining why DipA is found more broadly in the fungal kingdom.

As putative homologues for PxdA were found only in the Pezizomycotina, we hypothesized that a cellular function for peroxisome hitchhiking may also be specific to these fungi. The plugging of septal pores by Woronin bodies, which are derived from peroxisomes, also occurs exclusively within the Pezizomycotina ascomycetes (Jedd, 2011). Additionally, previous work has suggested that Woronin bodies might require active transport to reach nascent septal assembly sites before budding from peroxisomes (Leonhardt *et al.*, 2017). We therefore sought to test whether peroxisome hitchhiking affected Woronin body localization and function in septal pore plugging in *A. nidulans*.

Characterization of Woronin body biogenesis and distribution in *A. nidulans*

To determine whether Woronin body function requires hitchhiking, we first needed to reliably distinguish peroxisomes and Woronin bodies from one another in live cells. We achieved this by quantifying the colocalization and co-occurrence of fluorescently tagged proteins that were either an essential Woronin body component or a peroxisome marker. We chose SspA and HexA as representative Woronin body proteins for *A. nidulans* based on their involvement in Woronin body formation and function, which has been most extensively studied in *N. crassa*, another member of the Pezizomycotina.

In *N. crassa*, the proteins WSC (Woronin sorting complex; SspA in *A. nidulans*) and Hex-1 (HexA in *A. nidulans*) are essential for Woronin body formation and function, respectively. Previous work has shown that peroxisomes begin developing Woronin bodies with the import of Hex-1 via its C-terminal peroxisome targeting signal (PTS1) (Jedd and Chua, 2000). After import, Hex-1 self-assembles into a dense crystalline core, the main structural component of the Woronin body (Jedd and Chua, 2000; Tenney *et al.*, 2000). The Hex-1 complex then polarizes to one side of the peroxisome due to

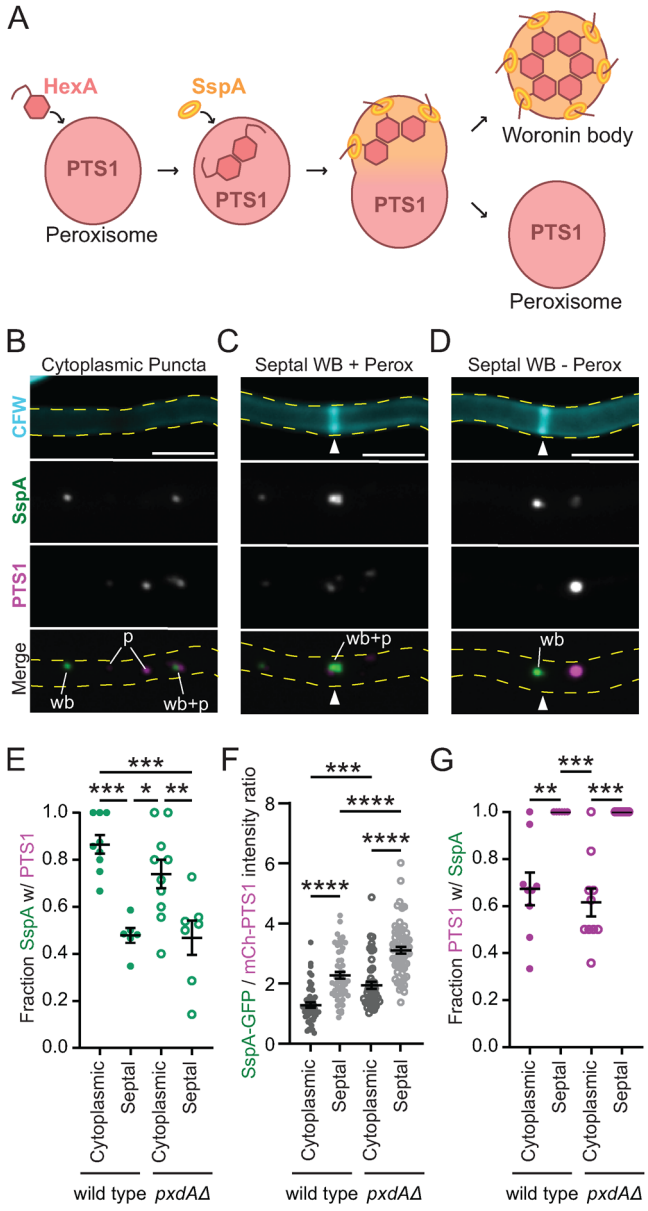

FIGURE 1: Characterization of Woronin body maturation from peroxisomes in the cytoplasm vs. at septa. (A) Diagram of Woronin body maturation from peroxisomes after import of HexA and SspA from the cytoplasm. (B–D) Example of SspA-mGFP5 and mCherry-PTS1 in the cytoplasm (B) and at tip apical septa (C and D) of adult wild-type hyphae (sum-Z projections). White triangles indicate septa. CFW = calcofluor white, cell wall dye; WB = Woronin body; p = peroxisome. Scale bars = 5 µm. (E) Average SspA-mGFP5 co-occurrence with mCherry-PTS1 while in the cytoplasm or associated with septa. Each dot represents one experiment with 5–20 ROIs scored (*n* fields of view, mean ± SD: wild type cytoplasmic = 9, 0.87 ± 0.12; wild type septal = 6, 0.48 ± 0.08; *pxdA*Δ cytoplasmic = 10, 0.74 ± 0.19; *pxdA*Δ septal = 7, 0.47 ± 0.019). (F) Average intensity ratio of SspA-mGFP5 and mCherry-PTS1 in puncta at septa and in the cytoplasm (n puncta, mean ± SD: wild type cytoplasmic = 49, 1.28 ± 0.63; wild type septal = 56, 2.28 ± 0.84; *pxdA*Δ cytoplasmic = 48, 1.94 ± 0.82; *pxdA*Δ septal = 62, 3.11 ± 0.89). (G) Average mCherry-PTS1 co-occurrence with SspA-mGFP5 in the cytoplasm or associated with septa. Each dot represents one experiment with 5–20 ROIs scored (*n* fields of view, mean ± SD: wild type cytoplasmic = 9, 0.67 ± 0.21; wild type septal = 6, 1.00 ± 0; *pxdA*Δ cytoplasmic = 10, 0.62 ± 0.19; *pxdA*Δ septal = 7, 1.00 ± 0). For E–G: Ordinary one-way analysis of variance (ANOVA) with post-hoc Tukey–Kramer test for multiple comparisons. Error bars represent SEM. $P > 0.05$ (labeled ns for "not significant," or not shown), $P \leq 0.05$ (*), $P \leq 0.01$ (**), $P \leq 0.001$ (***), $P \leq 0.0001$ (****).

the presence of the WSC protein in the peroxisome membrane (Liu *et al.*, 2008). This polarization is followed by organelle fission and separation of the Woronin body from the peroxisome (Tey *et al.*, 2005; Escaño *et al.*, 2009).

The formation of Woronin bodies in *A. nidulans* is largely similar to that of *N. crassa*, as they also mature from peroxisomes following the import of HexA and SspA (Figure 1A) (Beck and Ebel, 2013; Dimou *et al.*, 2019). To characterize the colocalization of Woronin bodies with peroxisomes in *A. nidulans*, we quantified the degree of overlap between endogenously tagged HexA, SspA, and the peroxisome marker PTS1 via fluorescence microscopy in freshly germinated conidia (germlings). We found that almost all SspA puncta had co-occurring HexA signal. On the other hand, a large population of HexA puncta had no corresponding SspA signal (Supplemental Figure S2, A and B). PTS1 co-occurred more frequently with HexA (Supplemental Figure S2, C and D) than it did with SspA (Supplemental Figure S2, E and F), suggesting that HexA is imported into peroxisomes before SspA. Consistent with this finding, PTS1 and HexA were often, but not always, closely overlapping (Supplemental Figure S2C), whereas PTS1 and SspA were often adjacent and only weakly overlapping with one another (Supplemental Figure S2E). Together, these data suggest that while the majority of peroxisome and Woronin body proteins exist within the same membrane-bound compartment, distinct stages of Woronin body maturation can be visualized using fluorescence microscopy.

These colocalization experiments in live cells established that SspA could serve as a bona fide marker for later stages of Woronin body maturation. We therefore used this as a tool to visually distinguish whether Woronin body (SspA-mGFP5) and peroxisome (mCherry-PTS1) colocalization varies at different intracellular positions in wild-type hyphae. We began by scoring the fraction of colocalized Woronin body and peroxisome puncta in the cytoplasm (Figure 1B) versus at septa (Figure 1, C and D). Cytoplasmic Woronin bodies were frequently associated with a peroxisome in wild type hyphae (Figure 1E) and rarely found without an attached peroxisome (Figure 1B). In comparison, at septa, about half of Woronin bodies had no associated peroxisome signal (Figure 1, D and E). For those septal Woronin bodies with a corresponding peroxisome signal, the Woronin body signal was always closer to the septa (Figure 1C, white arrow). This preferred orientation is likely due to Woronin body tethering at septal sites by HexA (Leonhardt *et al.*, 2016).

To estimate the relative amounts of peroxisome versus Woronin body proteins in the cytoplasm and at septa, we quantified the fluorescence intensity of SspA and HexA relative to PTS1. The ratio of SspA to HexA was consistent at both septa and in the cytoplasm (Supplemental Figure S2G), suggesting that Woronin body composition does not vary much between the two locations. In contrast, septal puncta exhibited a significantly higher intensity ratio of SspA to PTS1 than cytoplasmic puncta (Figure 1F). We observed a similar pattern for the ratio of HexA to PTS1 (Supplemental Figure S2H). Together, the data support the idea that most Woronin bodies have separated from peroxisomes by the time they associate with septa.

Finally, we wanted to estimate how many cytoplasmic peroxisomes were actively developing Woronin bodies. We observed that 67% of all cytoplasmic peroxisomes had an associated Woronin

body (Figure 1G). Overall, these data show that not all peroxisomes in the cytoplasm are actively developing Woronin bodies in *A. nidulans*. However, for peroxisomes that have begun developing Woronin bodies, the two organelles remain attached in the cytoplasm and separate only shortly before or immediately following recruitment to septa.

Previous work has established that in most Pezizomycotina including *A. nidulans*, Woronin bodies are tethered at septa (Momany *et al.*, 2002). However, a small number of species including *N. crassa* use a divergent mechanism of Woronin body tethering, whereby Woronin bodies are delocalized from septa and instead are tethered to the actin cortex throughout a hyphal compartment (Ng *et al.*, 2009). Our observations in *A. nidulans* on the localization of Woronin body maturation and separation from peroxisomes after septal association are similar to what was previously reported for *N. crassa* (Ng *et al.*, 2009), despite these species exhibiting different Woronin body localization and tethering mechanisms.

Woronin bodies move bidirectionally using the peroxisome hitchhiking protein PxdA

Woronin body biogenesis is thought to occur primarily in the cytoplasm near the hyphal apex (Momany *et al.*, 2002; Tey *et al.*, 2005). Woronin bodies are then localized to their tethering site at or near septa, where they function to seal septal pores following injury (Leonhardt *et al.*, 2017). However, the mechanism by which they are transported to septa is unknown. We therefore wanted to characterize Woronin body movement in hyphae and determine whether peroxisome hitchhiking was responsible for Woronin body movement and transport to septa.

We showed that Woronin bodies frequently colocalize with peroxisomes in the cytoplasm but are present alone at septa (Figure 1E). This suggests that Woronin bodies could either 1) move in conjunction with hitchhiking peroxisomes and bud off once present at septa or 2) bud off peroxisomes in the cytoplasm and be transported to septa by a distinct mechanism. To test this, we first compared Woronin body and peroxisome movement in adult hyphae. In *A. nidulans*, only a small population of peroxisomes exhibit long-distance movements at a given time (Egan *et al.*, 2012; Salogiannis *et al.*, 2016). We found that Woronin bodies also exhibit infrequent but dynamic bidirectional movements, like peroxisomes (Supplemental Movie S1). We observed that 10% of total movements for both peroxisomes and Woronin bodies were processive over long distances (>3 μm), indicative of microtubule-driven transport. During these long-distance movements, Woronin bodies moved at similar speeds (Figure 2A) and over similar distances as peroxisomes (Figure 2B). Both peroxisomes and Woronin bodies also exhibited bidirectional movements with no directional bias (Figure 2C). This characterization of Woronin body motility closely matched previously published results for peroxisome hitchhiking in *A. nidulans* (Egan *et al.*, 2012; Salogiannis *et al.*, 2016).

Next, we sought to test how frequently Woronin bodies and peroxisomes colocalize during long-distance runs (>3 μm traveled in one direction). The large majority of moving Woronin bodies were colocalized with a peroxisome, and vice versa (Figure 2, D and E). This finding was surprising as we previously observed that only two thirds of cytoplasmic peroxisomes had associated Woronin body signal (Figure 1G). Furthermore, we found no obvious bias in whether the Woronin body was "leading" or "trailing" the peroxisome during motile runs and instead observed that the signals frequently overlapped during movement (Figure 2F). This contrasts with our observations on stationary cytoplasmic peroxisomes and Woronin bodies, which frequently exhibited Woronin body signal that was polarized and offset to one side of the peroxisome signal (Figure 1B). Together, these data suggest that Woronin body proteins move via association with a hitchhiking peroxisome, and not as a separate/distinct organelle.

We next set out to determine whether Woronin body movement required the essential peroxisome hitchhiking protein PxdA. Compared to wild-type hyphae, in which peroxisomes and Woronin bodies are consistently distributed across hyphae (Figure 2G), *pxdA*Δ hyphae had an accumulation of both peroxisomes and Woronin bodies at the hyphal tip (Figure 2H) and a drastic reduction in the number of Woronin bodies and peroxisomes moving in either direction (Figure 2C; Supplemental Movie S2). Furthermore, motile Woronin bodies colocalized with the putative hitchhiking tether PxdA (Figure 2, I and J). These data demonstrate that Woronin bodies require PxdA for long-distance, bidirectional movements in hyphal tips.

While loss of PxdA abolished most long-distance Woronin body movements, a small number of Woronin bodies still moved processively in *pxdA*Δ hyphal tips (Supplemental Figure S2, K and L). However, these Woronin bodies were still colocalized with peroxisomes during this movement (Figure 2E). Additionally, the overall Woronin body and peroxisome co-occurrence (SspA/PTS1) in *pxdA*Δ hyphae was similar to what was observed in wild type (Figure 1, E–G, and Supplemental Figure S2, F and J). These findings demonstrate that the majority of Woronin body movement occurs via association with hitchhiking peroxisomes and that PxdA is not important for the assembly of Woronin bodies.

Essential Woronin body proteins are not required for peroxisome hitchhiking

As Woronin bodies and peroxisomes comigrated during long-distance runs and most motile peroxisomes colocalized with Woronin bodies while moving (Figure 2E), we wondered whether the presence of Woronin body proteins was required for peroxisome motility. We examined this using mutants lacking either HexA or SspA (Supplemental Figure S3A). Loss of HexA or SspA did not significantly affect the average number of moving peroxisomes per cell (Supplemental Figure S3B). In *hexA*Δ hyphae, peroxisomes showed a slight accumulation at hyphal tips (Supplemental Figure S3C) but to a lesser extent than the accumulation observed in *pxdA*Δ hyphae (Supplemental Figure S3D). Despite nearly all moving peroxisomes possessing Woronin body proteins, these data show that the ability to form Woronin bodies is not required for peroxisome hitchhiking.

Woronin bodies localize at septa and plug damaged hyphae independently of hitchhiking

We next wanted to test whether peroxisome–Woronin body hitchhiking is required for Woronin bodies to localize to septa in undamaged hyphae. First, we quantified the cytoplasmic localization of Woronin bodies in strains lacking peroxisome movement (*pxdA*Δ and *hookA*Δ), as well as in a strain with nonfunctional Woronin bodies (*hexA*Δ). We included *hookA*Δ because HookA is the adaptor protein that links microtubule motors to early endosomes in *A. nidulans* (Zhang *et al.*, 2014) and loss of HookA therefore disrupts both early endosome and peroxisome distribution and motility (Salogiannis *et al.*, 2016). As predicted, loss of peroxisome movement in both *pxdA*Δ and *hookA*Δ hyphae results in accumulation of SspA-labeled Woronin bodies at the hyphal tip (Figure 3, A and B). There were occasionally very bright Woronin bodies at the apex of wild-type hyphal tips, corresponding to a slight peak in intensity around 0.5 μm from the apex (Figure 3B, black line), which was abolished in

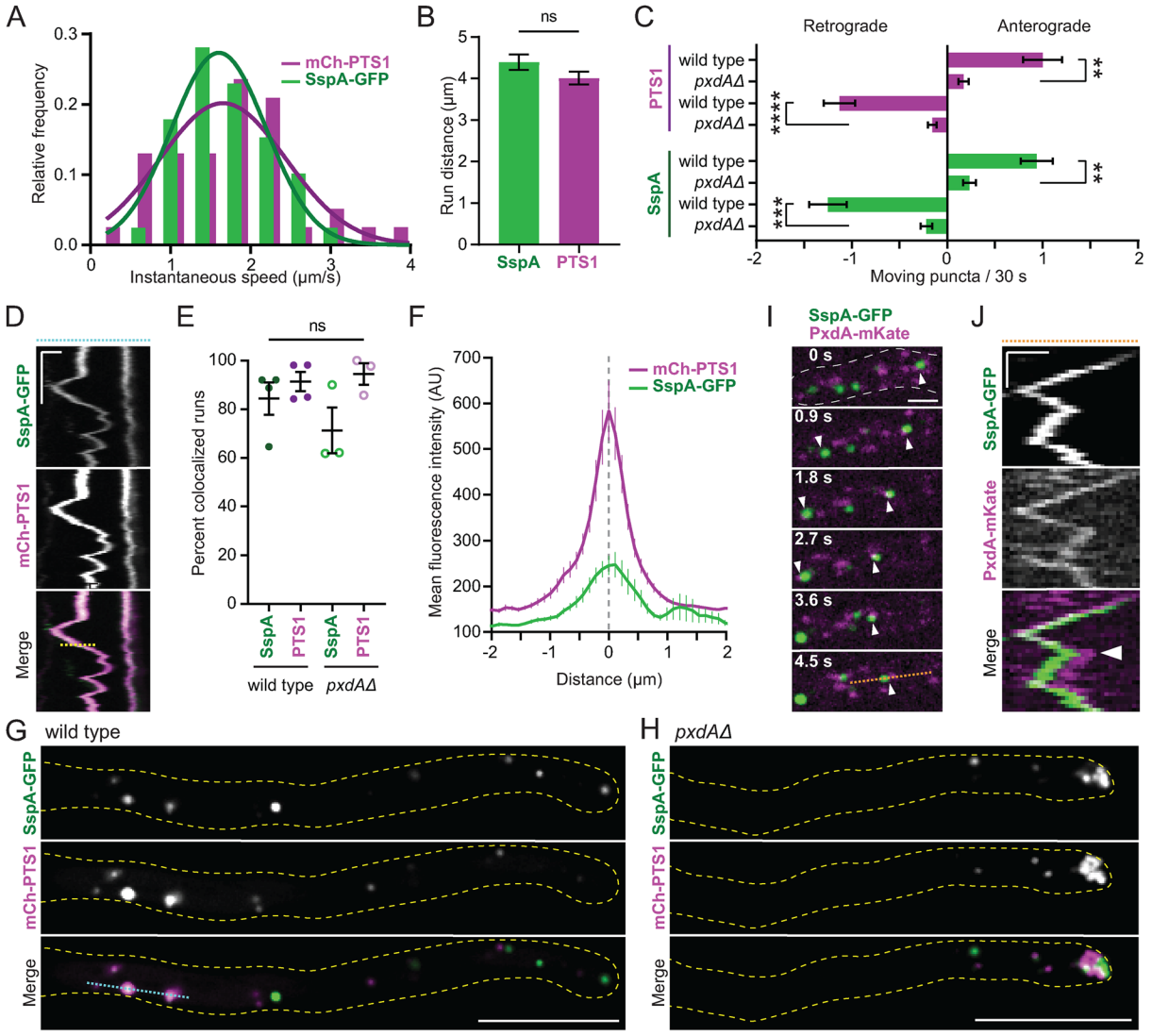

FIGURE 2: Woronin bodies at the hyphal tip exhibit dynamic, bidirectional movement with peroxisomes, and this movement requires PxdA. (A) Histogram of speeds of long-distance runs (>3 μm traveled in one direction) for SspA-mGFP5 and mCherry-PTS1 puncta (*n* directed runs/total, mean ± SD: SspA-mGFP5 = 39/390, 1.71 ± 0.59 μm/s; mCherry-PTS1 = 34/330, 1.72 ± 0.79 μm/s). Solid lines indicate nonlinear Gaussian fit lines (SspA-mGFP5: $R^2 = 0.95$; mCherry-PTS1: $R^2 = 0.76$). (B) Mean distance of long-distance runs for SspA-mGFP5 and mCherry-PTS1 (*n*, mean ± SD: SspA-mGFP5 = 39 runs, 4.39 ± 1.2 μm; mCherry-PTS1 = 34 runs, 4.01 ± 0.96 μm). (C) Number of anterograde (toward the hyphal tip) and retrograde (toward the apical septum) movements of mCherry-PTS1 (top) and SspA-mGFP5 (bottom) in wild-type and *pxdA*Δ adult hyphae (*n*: wild type = 32 cells and *pxdA*Δ = 64 cells. PTS1 mean ± SD puncta/30 s: anterograde wild type = 1.0 ± 1.2; anterograde *pxdA*Δ = 0.17 ± 0.42; retrograde wild type = –1.1 ± 0.94; retrograde *pxdA*Δ = –0.16 ± 0.37. SspA mean ± SD: anterograde wild type = 0.94 ± 0.95; anterograde *pxdA*Δ = 0.23 ± 0.53; retrograde wild type = –1.25 ± 1.1; retrograde *pxdA*Δ = –0.19 ± 0.50). (D) Kymograph depicting mCherry-PTS1 and SspA-mGFP5 colocalization over time. This kymograph was generated by the blue dashed line shown in G. The yellow dashed line is an example of a line used for panel F. X-scale bar = 1 μm, Y-scale bar = 10 s. (E) Percentage of long-distance runs (>3 μm) that are colocalized; each dot represents an individual experiment, where all runs from at least 10 hyphal tips were scored for colocalization. The number of moving SspA puncta ranged from 11 to 18 for *pxdA*Δ and from 14 to 30 for wild-type experiments. The number of moving PTS1 puncta ranged from 6 to 13 for *pxdA*Δ and from 7 to 26 for wild-type experiments (*n* experiments, mean ± SD: wild-type SspA = 4, 0.84 ± 0.13; wild-type PTS1 = 4, 0.91 ± 0.08; *pxdA*Δ SspA = 3, 0.71 ± 0.16; *pxdA*Δ PTS1 = 3, 0.95 ± 0.08). (F) Mean intensity of SspA-mGFP5 and mCherry-PTS1 during comigrating runs in wild type (*n* = 53 runs collected from 23 cells). The gray dashed line indicates the middle of the mCherry-PTS1 peak. (G, H) SspA-mGFP5 and mCherry-PTS1 in a single plane of wild-type (G) and *pxdA*Δ (H) hyphal tips. The blue dashed line was used to generate kymograph in D. Scale bars = 10 μm. (I) SspA-mGFP5 and PxdA-mKate comigration toward a growing hyphal tip (not shown; to the left). White arrows indicate two comigration events. The dashed yellow line in the last panel was used to generate the kymograph in I. Scale bar = 2 μm. (J) Kymograph depicting SspA-mGFP5 and PxdA-mKate colocalization over time. X-scale bar = 1 μm, Y-scale bar = 3 s. White arrow indicates the time point at around 6 s where PxdA-mKate switches from leading SspA-mGFP5 to following. For B, C, and E: Error bars represent SEM. Unpaired *t* test; $P > 0.05$ (labeled ns for "not significant," or not shown), $P \leq 0.01$ (**), $P \leq 0.001$ (***), $P \leq 0.0001$ (****).

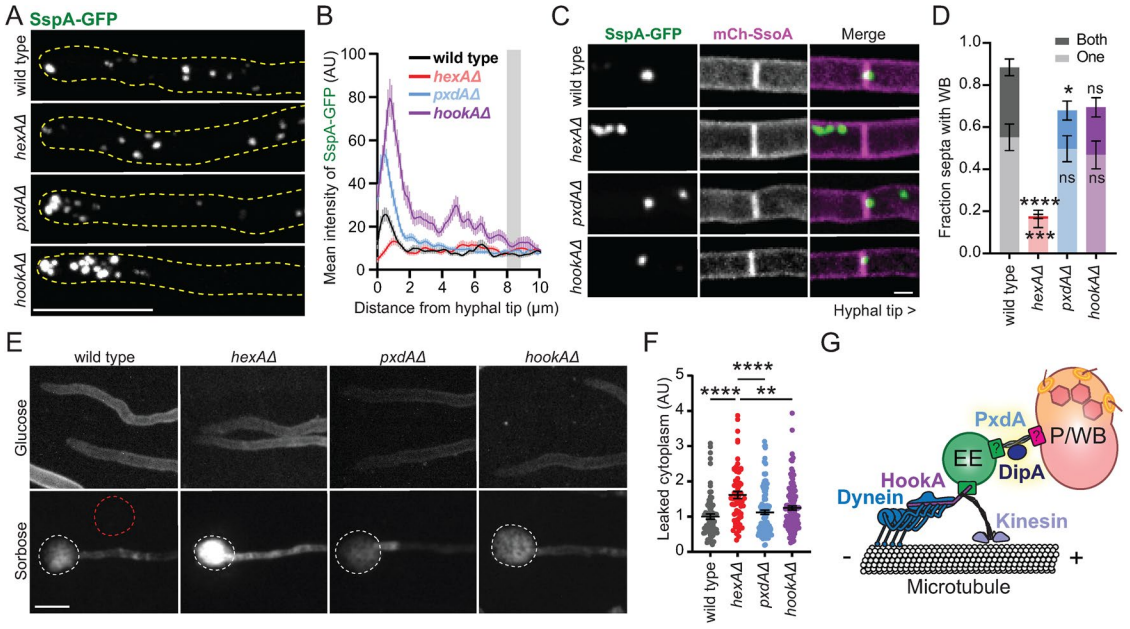

FIGURE 3: Woronin body hitchhiking is not required for localization to septa or septal plugging after hyphal damage. (A) SspA-mGFP5 localization at the hyphal tip in adult hyphae (max-Z projections). Scale bar = 10 μm. (B) Mean intensity of SspA-mGFP5 from the hyphal tip inward (*n* hyphae: wild type = 140; *hexA*Δ = 92; *pxdA*Δ = 225; *hookA*Δ = 132). Gray bar indicates approximate position of a tip apical nucleus. (C) Association of Woronin bodies at tip apical septa when grown in glucose MM (max-Z projections). Hyphal tips would be to the right of each image. Scale bar = 2 μm. (D) Fraction apical septa with Woronin bodies, quantified as being on one side (lighter bars; bottom) or both sides (darker bars; top) of septa. Each experiment scored 8–64 apical septa (*n* experiments, mean ± SD: one side wild type = 7, 0.55 ± 0.17; one side *hexA*Δ = 8, 0.16 ± 0.12; one side *pxdA*Δ = 6, 0.50 ± 0.15; one side *hookA*Δ = 4, 0.47 ± 0.13; both sides wild type = 7, 0.32 ± 0.12; both sides *hexA*Δ = 8, 0.012 ± 0.027; both sides *pxdA*Δ = 6, 0.18 ± 0.11; both sides *hookA*Δ = 4, 0.23 ± 0.092). (E) Hyphae expressing mCherry-SsoA as a cell membrane marker, when grown in 1% glucose agar vs. 2% sorbose/0.1% glucose agar (sum-Z projections). Scale bar = 10 μm. The white circles indicate leaked cytoplasm due to hyphal tip bursting, and the red circle is an example of a background fluorescence measurement. (F) Leaked cytoplasm, measured as the integrated density – (background * area) to correct for background intensity and then normalized to the average wild type (*n* burst cells, mean ± SD: wild type = 73, 1.00 ± 0.64; *hexA*Δ = 63, 1.61 ± 0.81; *pxdA*Δ = 125, 1.12 ± 0.67; *hookA*Δ = 119, 1.25 ± 0.65). (G) Model of peroxisome (P) and Woronin body (WB) hitchhiking on early endosomes (EE). For D and F: Error bars represent SEM. Ordinary one-way ANOVA with post-hoc Tukey–Kramer test; $P > 0.05$ (labeled ns for "not significant"), $P \leq 0.05$ (*), $P \leq 0.01$ (**), $P \leq 0.001$ (***), $P \leq 0.0001$ (****).

*hexA*Δ hyphae (Figure 3B, red line). This peak in SspA intensity in wild-type tips could correspond to higher levels of SspA import into peroxisomes in this region or the presence of larger Woronin body/peroxisome organelles that have not yet undergone fission.

We next examined Woronin body localization at tip apical septa in undamaged, wild-type hyphae as well as *pxdA*Δ, *hookA*Δ, *and hexA*Δ mutants. We chose tip apical septa because these septa were most recently formed (Kaminskyj, 2000) and are still capable of dynamically opening and closing via septal plugging (Bleichrodt *et al.*, 2012). Transmission electron microscopy studies in *A. nidulans* have previously reported between four and nine Woronin bodies at septa (Momany *et al.*, 2002). In assessing Woronin body localization at septa via fluorescence microscopy, three classes of Woronin body localization were identified: 1) septa with Woronin body signal on either side likely representing more than one Woronin body, 2) septa with Woronin body signal on only one side, and 3) no Woronin body signal (Supplemental Figure S4, A and B).

Manual scoring of these localization patterns revealed that most tip apical septa had Woronin bodies on one or both sides in wild-type hyphae (Figure 3, C and D). Furthermore, approximately one third of tip apical septa had Woronin bodies on both sides in wild-type hyphae (Figure 3D). As expected, most *hexA*Δ hyphae lacked Woronin bodies at apical septa. Both *pxdA*Δ and *hookA*Δ hyphae had an intermediate phenotype, with a slight reduction in the number of septa with Woronin bodies on both sides but similar numbers of septa with Woronin bodies on one side compared with wild type. This finding suggests that PxdA-mediated hitchhiking could contribute to achieving Woronin body localization on both sides of nascent septa. However, fluorescence measurements show that there is no significant difference in SspA signal at septa in wild-type versus *pxdA*Δ or *hookA*Δ hyphae (Supplemental Figure S4C). Overall, our data suggest that Woronin body localization at septa does not depend on Woronin body hitchhiking. Though Woronin body hitchhiking may have a minor contribution to Woronin body recruitment at septa, it is not the primary mechanism by which these organelles localize at septa. Woronin bodies in *pxdA*Δ hyphae could be recruited to tip apical septa by other mechanisms, such as cytoplasmic movement via "poleward drift" (Lin *et al.*, 2016) or passive association with septal assembly sites that are marked as the hyphal tip grows (Kaminskyj, 2000).

Finally, we wanted to test whether Woronin body hitchhiking was important for Woronin body–based sealing of septal pores following hyphal damage. Growth on sorbose media induced tip lysis in just under half of cells, regardless of genotype (Supplemental Figure S4D). Tip lysis and cytoplasmic puddling were clearly visible on sorbose media for all strains (Figure 3E). The amount of leaked

protein was higher in lysed *hexA*Δ than in lysed wild-type, *pxdA*Δ, or *hookA*Δ cells (Figure 3F), despite subtle changes in total leakage area (Supplemental Figure S4E). This pattern of cytoplasmic leakage was recapitulated when dried mycelia were exposed to hypotonic shock via distilled water (Supplemental Figure S4F). Together, these data demonstrate that Woronin body hitchhiking is not required for proper septal plugging after hyphal damage.

Concluding thoughts

In this study, we found that peroxisome-derived organelles called Woronin bodies hitchhike on early endosomes in the filamentous fungus *A. nidulans.* Filamentous fungi open and close septal pores between adjacent cells to regulate intercellular communication, either during regular growth or in response to various stresses. Woronin bodies physically plug septal pores after cell wall damage to prevent uncontrolled cytoplasmic leakage throughout these interconnected hyphal cells (Pieuchot and Jedd, 2012). Woronin bodies have previously been described to move long distances in some filamentous fungi (*Zymoseptoria tritici* [Steinberg *et al.*, 2017]; *Aspergillus fumigatus* [Leonhardt *et al.*, 2017]; *A. nidulans* [Shen *et al.*, 2014; Dimou *et al.*, 2019]). However, the mechanism by which Woronin bodies move long distances and how that movement is linked to their function in septal pore blocking was unclear. We demonstrated that Woronin bodies move dynamically and bidirectionally by hitchhiking on PxdA-labeled early endosomes in *A. nidulans* (Figure 3G). We showed that Woronin bodies colocalize and mature while associated with peroxisomes in the cytoplasm. Additionally, we characterized the long-distance movements of both peroxisomes and Woronin bodies and showed that the movement of both organelles requires PxdA- and HookA-mediated transport of early endosomes.

Despite undergoing dynamic movements throughout the cytoplasm, we found that Woronin body hitchhiking is not required for their localization at septal pores or their function in septal blocking after damage. It was previously suggested that following biogenesis at the growing hyphal apex, Woronin bodies undergo retrograde transport toward septal tethering sites (Momany *et al.*, 2002; Tey *et al.*, 2005). Mutants that lack the ability to optimally localize Woronin bodies at septa, or at cortical tethers in species like *N. crassa*, are unable to immediately occlude septal pores following injury (Liu *et al.*, 2008; Dimou *et al.*, 2019). Therefore, we hypothesized that Woronin body movement via hitchhiking would be required for Woronin body localization at septa and important for septal plugging. Instead, we find that Woronin bodies do not require PxdA-mediated hitchhiking or HookA-mediated dynein–driven transport to reach or associate with septa. While the mechanism of their septal localization is still unclear, one possibility is that Woronin bodies associate with septa by passively diffusing past septal assembly sites that are defined during hyphal growth (Kaminskyj, 2000). Our data support this model because in two mutants where Woronin body motility and cytoplasmic distribution are affected (*pxdA*Δ and *hookA*Δ), we still observe Woronin bodies localizing at septa. Conversely, there could be some other mechanism of transport that Woronin bodies utilize to reach septa that has not yet been discovered. Within the Pezizomycotina, different mechanisms of septal plugging can operate either redundantly with or independently from Woronin bodies. This includes septal-associated proteins such as SOFT (Fleißner and Glass, 2007; Tsukasaki *et al.*, 2016), highly disordered or spontaneously gelling proteins (Lai *et al.*, 2012; Mamun *et al.*, 2020, 2023), and other proteins that localize at septa via mitotic regulation (Shen *et al.*, 2014).

While our study has identified that Woronin body motility is not required for its positioning or function in *A. nidulans*, the importance of Woronin body hitchhiking might differ in other fungal species. In *N. crassa*, for example, Woronin bodies do not associate with septa and instead are tethered to the actin cortex along the cellular periphery (Ng *et al.*, 2009). It is therefore possible that hitchhiking might play a role in Woronin body positioning or function in septal plugging in species like *N. crassa*. The function of Woronin bodies in septa plugging is also important for virulence of many pathogenic ascomycetes, including the rice blast fungus *Magnaporthe grisea* (Soundararajan *et al.*, 2004), the entomopathogenic fungus *Metarhizium robertsii* (Tang *et al.*, 2020), and the head blight fungus of cereal grains *Fusarium graminearum* (Zheng *et al.*, 2013; Zhang *et al.*, 2019). Understanding the mechanisms by which Woronin bodies form, move, and function is therefore potentially important for the development of treatments for these high-priority fungal pathogens.

The physiological role of peroxisome hitchhiking remains open. Currently, *U. maydis* is the only species other than *A. nidulans* in which peroxisomes have been demonstrated to hitchhike on early endosomes (Guimaraes *et al.*, 2015). This hitchhiking behavior appears to be PxdA independent, as we were unable to identify a PxdA homologue in *U. maydis*. Basidiomycete fungi such as *U. maydis* do not use Woronin body–mediated septal plugging, further suggesting that peroxisome hitchhiking has a physiological function outside of septal plugging. Future work will involve deciphering roles of peroxisome hitchhiking that are general or specific to different clades of filamentous fungi.

MATERIALS AND METHODS

Request a protocol through *Bio-protocol*.

Strain construction

A. nidulans strains used in this study are listed in Supplemental Table S2. New strains were generated by transforming PCR-amplified targeting DNA into *A. nidulans* protoplasts (Szewczyk *et al.*, 2006) or via genetic crosses (Todd *et al.*, 2007). The genotypes of novel strains were confirmed by PCR amplification from isolated genomic DNA (Lee and Taylor, 1990) and Sanger sequencing.

Plasmid cloning

Plasmids and primers generated for this study are listed in Supplemental Tables S3 and S4, respectively. All DNA constructs were designed for homologous recombination at the endogenous locus with the endogenous promoter unless otherwise stated. Novel plasmids were cloned using Gibson isothermal assembly (Gibson *et al.*, 2009; Rabe and Cepko, 2020). Briefly, fragments were amplified using PCR (NEB Q5 high-fidelity DNA polymerase, M0491) from other plasmids or *A. nidulans* genomic DNA. Then, fragments were assembled into the Blue Heron Biotechnology pUC vector at the 5′*Eco*RI and 3′*Hin*dIII restriction sites. The cloning of *mTagGFP2-rabA::AfpyrG*, *mCherry-FLAG-PTS1::AfpyroA*, and *2xBFP-PTS1::AfriboB* were described previously (Tan *et al.*, 2014). The cloning of *pxdA-mKate2::AfpyroA* and *pxdA*Δ*::AfriboB* were also previously published (Salogiannis *et al.*, 2016, 2021). All fluorescently tagged proteins had a GA5 linker. The sequence for mGFP5 was optimized for expression in *Arabidopsis thalania* plants (Siemering *et al.*, 1996).

Fungal growth conditions

A. nidulans strains were grown in either liquid or solid agar containing yeast-glucose (YG) complete media or minimal media (MM) (Szewczyk *et al.*, 2006). YG and MM agar plates contained 10 g/l agar-agar/gum agar (USB 10654). YG complete media contained

Bacto yeast extract (5 g/l), 2% final D-glucose (20 g/l), trace elements solution (2 ml/l), uracil (56 mg/l), uridine (122.1 mg/l), and riboflavin (2.5 mg/l). The trace elements stock solution (500×) contained $FeSO_4 \cdot 7H_2O$ (1 g/l), $ZnSO_4 \cdot 7H_2O$ (8.8 g/l), $CuSO_4 \cdot 5H_2O$ (0.4 g/l), $MnSO_4 \cdot H_2O$ (0.15 g/l), $Na_2B_4O_7 \cdot 10H_2O$ (0.1 g/l), and $(NH_4)_6Mo_7O_{24} \cdot 4H_2O$ (0.05 g/l). Regular MM contained 1% final D-glucose (10 g/l), $MgSO_4$ (2 ml/l 26% wt/vol), trace elements solution (2 ml/l), and stock salt solution (10 ml/l). Sorbose MM, to induce hyphal tip lysis (Soundararajan *et al.*, 2004), contained 2% final L-sorbose (20 g/l), 0.1% final D-glucose (1 g/l), trace elements solution (2 ml/l), and stock salt solution (10 ml/l). The stock salt solution (100×; pH 6–6.5) contained $NaNO_3$ (60 g/l), KCl (5.2 g/l), and KH_2PO_4 (15.2 g/l). For strains with auxotrophic alleles, MM was supplemented as follows: *pyrG89* allele: 0.5 mM uracil and 0.5 mM uridine; *pabaA1* allele: 1.46 µM *p*-aminobenzoic acid; *riboB2* allele: 6.6 µM riboflavin; *pyroA4* allele: 3.0 µM pyridoxine.

To grow adult hyphae for imaging, spores were inoculated into MM agar with supplements and incubated for 16–20 h at 37°C. Individual colonies were cut from the agar and inverted onto 35 mm #1.5 glass-bottom imaging dishes (Cellvis D35C4201.5N). To grow germlings for imaging, spores were collected into 0.01% Tween-80 (Sigma-Aldrich P1754) and their density was measured using a hemocytometer. The spores were then inoculated into liquid MM with supplements at a density of 5×10^5 spores/ml in a four-chamber, 35 mm dish and incubated for 16–20 h at 30°C in an unsealed humid plastic container.

Phylogenetic analysis of peroxisome hitchhiking

Pezizomycotina fungi included in this analysis were previously published to have Woronin bodies and/or have been referenced as representatives of different clades (Nguyen *et al.*, 2017; Prostak *et al.*, 2021). Species were included only if they had their whole genome sequenced and proteome annotated and/or drafted at the time of this analysis (30 August 2022). The phylogenetic tree for fungi was drawn manually based on the taxonomic rankings of each species on NCBI.

Homologous genes for PxdA (AN1156) and DipA (AN10946) were identified using BLASTp available at NCBI (https://blast.ncbi.nlm.nih.gov/) (parameters: $E = 1.0 \times 10^{-5}$, word size of 6, BLOSUM62 matrix, gap costs existence 11 and extension 1, filtering low complexity regions, minimum percent coverage 20%). Reciprocal BLASTs were used to confirm all candidate homologues. The reference proteins database (refseq_proteins) was used to reduce redundancy of search results. For species where the refseq_proteins database was unavailable, the nonredundant protein sequences database (nr) was used instead. The E value, query coverage, and percent identity of the top hits for a reference strain of each species were recorded (Supplemental Table S1).

To identify PxdA homologues, three query sequences were used: the PxdA coiled-coil region, previously defined as CC1-3 (amino acids [aa] 1466–2115); the PxdA uncharacterized N-terminus (aa 1–1465); and the full-length PxdA protein (aa 1–2236) [Salogiannis *et al.*, 2016]. The conserved stretch of amino acids in the PxdA CC3 domain is aa 2034–2058. The amino acid consensus logo diagram (Supplemental Figure S1D) was made by first aligning all identified PxdA homologues in SnapGene software (Windows version 6.1.1) using MUSCLE multiple protein sequence alignments (version 3.8.1551, default parameters). The aligned conserved amino acid stretch was then used as an input for WebLogo 3 (https://weblogo.threeplusone.com/; version 3.7.12). The coiled-coil regions of all PxdA homologues were individually predicted by querying each sequence in the Waggawagga coiled-coil prediction software (https://waggawagga.motorprotein.de/) with the following settings: Marcoil, Scorer 2.0 oligomerization, and window length of 21.

PxdA possesses a predicted coiled-coil region that is necessary and sufficient for peroxisome hitchhiking (Salogiannis *et al.*, 2016). The coiled-coil prediction software Waggawagga estimated between three and six distinct coiled-coils in each PxdA homologue, with the total coiled-coil region varying from 167 to 307 aa long (Supplemental Table S1). All PxdA homologues possessed an N-terminal extension of variable length with no discernible conserved domains, based on NCBI and PFAM databases.

For identifying DipA homologues, query sequences included both the full-length DipA protein (aa 1–704) and the DipA metallophosphatase domain alone (aa 45–96). DipA homologues were defined to have a metallophosphatase domain followed by a conserved domain of unknown function (DUF2433). The amino acid boundaries of both the metallophosphatase and DUF2433 domains were identified for all DipA homologues using NCBI domain prediction and MUSCLE multiple protein sequence alignments to the *A. nidulans* DipA reference sequence in SnapGene.

Spinning-disk confocal microscopy

Live cell imaging was performed at room temperature using a Nikon Ti2 microscope mounted with a Yokogawa W1 spinning-disk confocal scan head and two Prime95B cameras (Photometrics). All images were acquired in 16-bit format. NIS Elements Advanced Research software (Nikon) was used to run the microscope with the 488 and 561 nm lasers of a six-line LUN-F-XL laser engine (405, 445, 488, 515, 561, and 640 nm). The stage *xy* position was controlled by a ProScan linear motor stage controller (Prior), and its *z* position was controlled by a piezo Nano-Z stage positioner (Mad City Labs). An Apo TIRF 100× 1.49 NA objective (Nikon) was used for all experiments except for the imaging of apical septa for hyphae grown in glucose and sorbose agar, which required an S Fluor 40× 1.30 NA objective (Nikon) to capture a larger field of view.

Simultaneous dual-color imaging was used to assess colocalization of Woronin body and peroxisome proteins in germlings. Z-stacks were collected to capture the complete volume of germling cells in the field of view (0.2 µm step size, 8–10 µm total depth). The 488 and 561 nm lines were used to excite mGFP5- and mCherry-tagged fusion proteins, respectively. The emission was split with a Cairn TwinCam with a 580LP filter. The GFP/488 emission was reflected and passed through a 514/30 bandpass filter onto camera 2. The mCherry/561 fluorescence was passed through a 617/73 and an additional 600/50 bandpass filter to camera 1. The cameras were aligned manually in NIS Elements using 0.1 µm TetraSpeck beads (ThermoFisher T14792). Image acquisition settings, such as exposure time and laser power, were determined at the beginning of each imaging session to eliminate fluorescence bleed through between each channel.

Triggered acquisition of 488/561 was used when imaging Woronin body association at apical septa with the 40× objective and when imaging SspA-mGFP5 comigration with PxdA-mKate with the 100× objective. The firing of the 488 and 561 nm lasers was synchronized by the Prime95B camera trigger signal, which was integrated into a Nikon BB connected to a 6723 DAQ board housed in an external Pxi chassis (National Instruments). A quad bandpass filter (Chroma ZET405/488/561/640mv2) was placed in the emission path of the W1 scan head.

Quantitative image analysis

All image analysis was performed using ImageJ/FIJI (National Institutes of Health, Bethesda, MD). All microscopy images were blinded before analysis using a custom script in R (R Core Team, 2021). All

macros (ImageJ, Windows version 1.53q) and data processing scripts (R, Windows version 4.1.0) are available on GitHub (https://github.com/LiviaSongster). Statistical tests were performed using GraphPad Prism (Windows version 9.4.1).

Colocalization and co-occurrence

To prepare Z-stacks for colocalization analysis, whole germlings were cropped, max-Z projected, and saved as separate files. For both the 488 and the 561 channels, a Gaussian Blur (sigma = 1) and background subtraction (rolling = 50) were applied before thresholding (Yen dark) to generate a binary puncta mask. The threshold for the green channel was set at 15–65535 and for the red channel at 20–65535. All gray values outside of that channel's mask were cleared to eliminate background. Colocalization was then quantified using Pearson's coefficient of correlation and Mander's coefficient of co-occurrence algorithms via the JACoP plug-in in ImageJ (Bolte and Cordelières, 2006; Aaron *et al.*, 2018).

The fraction of SspA puncta with PTS1 and the fraction of SspA puncta with PTS1 were manually scored for four separate experiments containing at least 10 germlings each. Germlings were imaged for 60 s (300 ms interval) with a single z-plane using simultaneous dual-color settings. Puncta in the cytoplasm or at septa were manually segmented as a region of interest (ROI) and scored as co-localized if there was a punctum from both channels that overlapped by >50% and if the mean gray value of the puncta of the opposite channel was at least 10% brighter than the background. Motile puncta were assessed by first generating kymographs, and for directed runs where a punctum traveled >2 µm, the co-occurrence of puncta in both channels was manually scored.

To measure the fluorescence intensity ratio of different proteins, puncta from sum Z projections of germlings were manually circled as ROIs. The gray value of all puncta was measured in both the 488 and the 561 channels, and the intensity ratio for each ROI was calculated as the mean gray value of the 488 channel divided by the mean gray value of the 561 channel.

Organelle flux

Total puncta movement was estimated from single-plane, triggered-acquisition movies (30 s total length, 300 ms interval, 100 ms exposure per laser). The puncta crossing a perpendicular line ~10 µm from the hyphal tip were manually counted.

Intensity profile during movement

The intensity along a line (1 pixel width) was measured during a directed run for both the 488 and the 561 channels. The line scans from multiple kymographs were compiled in R. For each line scan, the maximum intensity in the 561 channel was set as x position 0 µm and then applied to the 488 channel.

Speed and distance traveled of migrating puncta

Adult hyphae were imaged for 60 s (300 ms interval) with a single z-plane using simultaneous dual-color settings. The line tool was used to trace puncta trajectories over time, and movies were re-sliced along these lines to generate kymographs. The instantaneous speed and run lengths of individual moving puncta were calculated from the inverse of the slopes of manual kymograph traces. A punctum was scored as moving if it exhibited a directed run (no pauses) >3 µm during its movement.

Hyphal tip line scans

Whole adult hyphae were imaged live as a Z-stack (0.2 µm step size, 8–10 µm total depth). Max-Z intensity projections of fluorescence micrographs were obtained, and the bright-field channel was used to trace from the hyphal tip inward using the segmented line tool (pixel width 20). The traces were superimposed on the fluorescence micrographs to project the average fluorescence intensity along the line. The mean background intensity was measured for each cell and subtracted from that cell's respective line scan before binning.

Woronin body localization at tip apical septa

Cells expressing mCherry-SsoA and SspA-mGFP5 were grown overnight with supplements in either regular MM (1% glucose) or sorbose MM (2% sorbose/0.1% glucose). Adult hyphae were imaged using the 40× objective to collect complete volume Z-stacks (0.2 µm step size, 8–10 µm total depth). Images were max-Z projected, and the apical septa were manually identified as ROIs and cropped. Crops of single septa were blinded, and Woronin body localization was manually scored as the fraction of apical septa with an associated Woronin body per experiment. The mean fluorescence intensity of SspA-mGFP5 from these max-Z projections was measured within a 0.5-µm-wide by 1-µm-long rectangle centered at an apical septum. The mean background intensity adjacent to each septum was measured and subtracted from the mean septal intensity. Background-corrected measurements were then normalized to the average septal intensity of wild type.

Cytoplasmic leakage

Cytoplasmic leakage was measured for burst hyphal tips in sorbose agar. First, complete Z stacks (0.2 µm step size, 4 µm total depth) were imaged, sum-Z projected, and blinded. The integrated density (mean intensity of puddle times puddle area) for each cytoplasmic puddle was measured in ImageJ and corrected by subtracting the product of the mean background intensity and puddle area. This background-corrected integrated density was then normalized to the mean observation for wild type to calculate the normalized amount of leaked cytoplasm.

As a complementary approach, mycelia were also subjected to hypotonic shock to induce global tip lysis, using a protocol for *A. nidulans* that was adapted from Fleißner and Glass (2007). Spores from strains expressing a cytoplasmic mTagGFP were inoculated into liquid YG media and grown overnight at 37°C. Mycelia were collected in Miracloth (EMD Millipore 475855) and dried with paper towels. Approximately 300 ± 10 mg of dried mycelia were submerged in 1 ml of sterile ddH_2O and vortexed to induce hypotonic damage at hyphal tips. Samples were spun at 15,000 × *g* for 1 min in a tabletop centrifuge to pellet cell debris, and the supernatant was diluted 1:10 in sterile ddH_2O for a 96-well microplate Bradford microassay (Bio-Rad 5000201) to estimate the amount of leaked protein. The absorbance at 595 nm was measured using a Cytation 5 plate reader (BioTek) and Gen5 data analysis software (Windows version 3.05).

ACKNOWLEDGMENTS

L.D.S. is funded by a National Science Foundation Graduate Research Fellowship Program and University of California, San Diego, Quantitative Integrative Biology T32 from the National Institutes of Health (NIH) (1T32GM127235). J.R.C. is funded by a MOSAIC award (K99/R00) from the NIH (K99GM140269). S.L.R-P. is supported by the Howard Hughes Medical Institute and the NIH (1R35GM141825). We thank John Salogiannis and Valentin Wernet for ideas and insight, Kaeling Tan for cloning RPB564, James Holcomb for cloning RPB2190, and Xin Xiang for the mGFP5 plasmid.

REFERENCES

Aaron JS, Taylor AB, Chew T-L (2018). Image co-localization—co-occurrence versus correlation. J Cell Sci 131, jcs211847.

Beck J, Ebel F (2013). Characterization of the major Woronin body protein HexA of the human pathogenic mold *Aspergillus fumigatus*. Int J Med Microbiol 303, 90–97.

Bleichrodt R-J, van Veluw GJ, Recter B, Maruyama J-I, Kitamoto K, Wösten HAB (2012). Hyphal heterogeneity in *Aspergillus oryzae* is the result of dynamic closure of septa by Woronin bodies. Mol Microbiol 86, 1334–1344.

Bolte S, Cordelières FP (2006). A guided tour into subcellular colocalization analysis in light microscopy. J Microsc 224, 213–232.

Christensen JR, Reck-Peterson SL (2022). Hitchhiking across kingdoms: cotransport of cargos in fungal, animal, and plant cells. Annu Rev Cell Dev Biol 6, 155–178.

Dimou S, Kourkoulou A, Amillis S, Percudani R, Diallinas G (2019). The peroxisomal SspA protein is redundant for purine utilization but essential for peroxisome localization in septal pores in *Aspergillus nidulans*. Fungal Genet Biol 132, 103259.

Egan MJ, Tan K, Reck-Peterson SL (2012). Lis1 is an initiation factor for dynein-driven organelle transport. J Cell Biol 197, 971–982.

Escaño CS, Juvvadi PR, Jin FJ, Takahashi T, Koyama Y, Yamashita S, Maruyama J-I, Kitamoto K (2009). Disruption of the Aopex11-1 gene involved in peroxisome proliferation leads to impaired Woronin body formation in *Aspergillus oryzae*. Eukaryot Cell 8, 296–305.

Fleißner A, Glass NL (2007). SO, a protein involved in hyphal fusion in *Neurospora crassa*, localizes to septal plugs. Eukaryot Cell 6, 84–94.

Gibson DG, Young L, Chuang R-Y, Venter JC, Hutchison CA, Smith HO (2009). Enzymatic assembly of DNA molecules up to several hundred kilobases. Nat Methods 6, 343–345.

Guimaraes SC, Schuster M, Bielska E, Dagdas G, Kilaru S, Meadows BRA, Schrader M, Steinberg G (2015). Peroxisomes, lipid droplets, and endoplasmic reticulum "hitchhike" on motile early endosomes. J Cell Biol 211, 945–954.

Harbauer AB, et al. (2022). Neuronal mitochondria transport Pink1 mRNA via synaptojanin 2 to support local mitophagy. Neuron 110, 1516–1531.e9.

Hirokawa N, Noda Y, Tanaka Y, Niwa S (2009). Kinesin superfamily motor proteins and intracellular transport. Nat Rev Mol Cell Biol 10, 682–696.

Jedd G (2011). Fungal evo-devo: organelles and multicellular complexity. Trends Cell Biol 21, 12–19.

Jedd G, Chua NH (2000). A new self-assembled peroxisomal vesicle required for efficient resealing of the plasma membrane. Nat Cell Biol 2, 226–231.

Kaminskyj SGW (2000). Septum position is marked at the tip of *Aspergillus nidulans* hyphae. Fungal Genet Biol 31, 105–113.

Lai J, Koh CH, Tjota M, Pieuchot L, Raman V, Chandrababu KB, Yang D, Wong L, Jedd G (2012). Intrinsically disordered proteins aggregate at fungal cell-to-cell channels and regulate intercellular connectivity. Proc Natl Acad Sci USA 109, 15781–15786.

Lee SB, Taylor JW (1990). 34—Isolation of DNA from fungal mycelia and single spores. In: PCR Protocols, San Diego: Academic Press, 282–287.

Leonhardt Y, Beck J, Ebel F (2016). Functional characterization of the Woronin body protein WscA of the pathogenic mold *Aspergillus fumigatus*. Int J Med Microbiol 306, 165–173.

Leonhardt Y, Kakoschke SC, Wagener J, Ebel F (2017). Lah is a transmembrane protein and requires Spa10 for stable positioning of Woronin bodies at the septal pore of *Aspergillus fumigatus*. Sci Rep 7, 44179.

Lin C, Schuster M, Guimaraes SC, Ashwin P, Schrader M, Metz J, Hacker C, Gurr SJ, Steinberg G (2016). Active diffusion and microtubule-based transport oppose myosin forces to position organelles in cells. Nat Commun 7, 11814.

Liu F, Ng SK, Lu Y, Low W, Lai J, Jedd G (2008). Making two organelles from one: Woronin body biogenesis by peroxisomal protein sorting. J Cell Biol 180, 325–339.

Luo K-R, Huang N-C, Chang Y-H, Yu T-S (2022). Arabidopsis cyclophilins direct plasmodesmata-targeting of mobile mRNA via organelle hitchhiking. Research Square, https://doi.org/10.21203/rs.3.rs-1088339/v1.

Mamun MAA, Cao W, Nakamura S, Maruyama J (2023). Large-scale identification of genes involved in septal pore plugging in multicellular fungi. Nat Commun 14, 1418.

Mamun MAA, Katayama T, Cao W, Nakamura S, Maruyama J (2020). A novel Pezizomycotina-specific protein with gelsolin domains regulates contractile actin ring assembly and constriction in perforated septum formation. Mol Microbiol 113, 964–982.

Momany M, Richardson EA, Van Sickle C, Jedd G (2002). Mapping Woronin body position in Aspergillus nidulans. Mycologia 94, 260–266.

Mouriño-Pérez RR (2013). Septum development in filamentous ascomycetes. Fungal Biol Rev 27, 1–9.

Ng SK, Liu F, Lai J, Low W, Jedd G (2009). A tether for Woronin body inheritance is associated with evolutionary variation in organelle positioning. PLoS Genet 5, e1000521.

Nguyen TA, Cissé OH, Yun Wong J, Zheng P, Hewitt D, Nowrousian M, Stajich JE, Jedd G (2017). Innovation and constraint leading to complex multicellularity in the Ascomycota. Nat Commun 8, 14444.

Oikawa K, Kasahara M, Kiyosue T, Kagawa T, Suetsugu N, Takahashi F, Kanegae T, Niwa Y, Kadota A, Wada M (2003). Chloroplast unusual positioning1 is essential for proper chloroplast positioning. Plant Cell 15, 2805–2815.

Olenick MA, Holzbaur ELF (2019). Dynein activators and adaptors at a glance. J Cell Sci 132, jcs227132.

Özkan N, Koppers M, van Soest I, van Harten A, Jurriens D, Liv N, Klumperman J, Kapitein LC, Hoogenraad CC, Farías GG (2021). ER–lysosome contacts at a pre-axonal region regulate axonal lysosome availability. Nat Commun 12, 4493.

Pieuchot L, Jedd G (2012). Peroxisome assembly and functional diversity in eukaryotic microorganisms. Annu Rev Microbiol 66, 237–263.

Prostak SM, Robinson KA, Titus MA, Fritz-Laylin LK (2021). The actin networks of chytrid fungi reveal evolutionary loss of cytoskeletal complexity in the fungal kingdom. Curr Biol 31, 1192–1205.

Rabe BA, Cepko C (2020). A simple enhancement for Gibson isothermal assembly. bioRxiv, https://doi.org/10.1101/2020.06.14.150979.

R Core Team (2021). R: a language and environment for statistical computing. Indianapolis, IN: R Foundation for Statistical Computing.

Reck-Peterson SL, Redwine WB, Vale RD, Carter AP (2018). The cytoplasmic dynein transport machinery and its many cargoes. Nat Rev Mol Cell Biol 19, 382–398.

Salogiannis J, Christensen JR, Songster LD, Aguilar-Maldonado A, Shukla N, Reck-Peterson SL (2021). PxdA interacts with the DipA phosphatase to regulate peroxisome hitchhiking on early endosomes. Mol Biol Cell 32, 492–503.

Salogiannis J, Egan MJ, Reck-Peterson SL (2016). Peroxisomes move by hitchhiking on early endosomes using the novel linker protein PxdA. J Cell Biol 212, 289–296.

Schinke J, Kolog Gulko M, Christmann M, Valerius O, Stumpf SK, Stirz M, Braus GH (2016). The DenA/DEN1 interacting phosphatase DipA controls septa positioning and phosphorylation-dependent stability of cytoplasmatic DenA/DEN1 during fungal development. PLoS Genet 12, e1005949.

Shen K-F, Osmani AH, Govindaraghavan M, Osmani SA (2014). Mitotic regulation of fungal cell-to-cell connectivity through septal pores involves the NIMA kinase. Mol Biol Cell 25, 763–775.

Siemering KR, Golbik R, Sever R, Haseloff J (1996). Mutations that suppress the thermosensitivity of green fluorescent protein. Curr Biol 6, 1653–1663.

Soundararajan S, Jedd G, Li X, Ramos-Pamploña M, Chua NH, Naqvi NI (2004). Woronin body function in *Magnaporthe grisea* is essential for efficient pathogenesis and for survival during nitrogen starvation stress. Plant Cell 16, 1564–1574.

Steinberg G, Schuster M, Hacker C, Kilaru S, Correia A (2017). ATP prevents Woronin bodies from sealing septal pores in unwounded cells of the fungus *Zymoseptoria tritici*. Cell Microbiol 19, e12764.

Szewczyk E, Nayak T, Oakley CE, Edgerton H, Xiong Y, Taheri-Talesh N, Osmani SA, Oakley BR (2006). Fusion PCR and gene targeting in *Aspergillus nidulans*. Nat Protoc 1, 3111–3120.

Tan K, Roberts AJ, Chonofsky M, Egan MJ, Reck-Peterson SL (2014). A microscopy-based screen employing multiplex genome sequencing identifies cargo-specific requirements for dynein velocity. Mol Biol Cell 25, 669–678.

Tang G, Shang Y, Li S, Wang C (2020). MrHex1 is required for Woronin body formation, fungal development and virulence in *Metarhizium robertsii*. J Fungi 6, 1–14.

Tegelaar M, Wösten HAB (2017). Functional distinction of hyphal compartments. Sci Rep 7, 6039.

Tenney K, Hunt I, Sweigard J, Pounder JI, McClain C, Bowman EJ, Bowman BJ (2000). hex-1, a gene unique to filamentous fungi, encodes the major protein of the Woronin body and functions as a plug for septal pores. Fungal Genet Biol 31, 205–217.

Tey WK, North AJ, Reyes JL, Lu YF, Jedd G (2005). Polarized gene expression determines Woronin body formation at the leading edge of the fungal colony. Mol Biol Cell 16, 2651–2659.
Titus MA (2018). Myosin-driven intracellular transport. Cold Spring Harb Perspect Biol 10, a021972.
Todd RB, Davis MA, Hynes MJ (2007). Genetic manipulation of *Aspergillus nidulans*: meiotic progeny for genetic analysis and strain construction. Nat Protoc 2, 811–821.
Tsukasaki W, Saeki K, Katayama T, Maruyama J-I, Kitamoto K (2016). Molecular dissection of SO (SOFT) protein in stress-induced aggregation and cell-to-cell interactive functions in filamentous fungal multicellularity. Fungal Biol 120, 775–782.
Zhang J, Qiu R, Arst HN Jr, Peñalva MA, Xiang X (2014). HookA is a novel dynein-early endosome linker critical for cargo movement *in vivo*. J Cell Biol 204, 1009–1026.
Zhang L, Liu C, Wang L, Sun S, Liu A, Liang Y, Yu J, Dong H (2019). FgPEX1 and FgPEX10 are required for the maintenance of Woronin bodies and full virulence of *Fusarium graminearum*. Curr Genet 65, 1383–1396.
Zheng Z, Gao T, Hou Y, Zhou M (2013). Involvement of the anucleate primary sterigmata protein FgApsB in vegetative differentiation, asexual development, nuclear migration, and virulence in *Fusarium graminearum*. FEMS Microbiol Lett 349, 88–98.